DOI: 10.48011/sbse.v1i1.2473

Fault Impedance Analysis in Half-Wavelength Transmission Lines

Javier Santiago Ortega*. Maria Cristina Tavares.*

** School of Electrical and Computer Engineering, University of Campinas (UNICAMP), Av. Albert Einstein, 400, 13083-250, Campinas, SP, Brazil (Phone: +55 19 35210258; e-mail: javiersa@dsce.fee.unicamp.br ; ctavares@unicamp.br).*

Abstract: Half-wavelength (HWL) line has excellent steady-state properties to power transmission over very long distances, and technical and economic advantages over HVDC very long lines. However, protection system based on impedance calculations need carefully attention due to specific behavior of HWL line under fault. This paper analyzes the fault impedance on HLW lines to produce more insight about the effect of the capacitance, the point of fault, the resonance phenomenon, the transmission line model and the phasor estimation to the impedance measurement process in protective devices. This paper shows that the phase impedance estimation suffers higher deviation from ideal values as faults are applied far away from terminals and transposition introduces an additional deviation. Three characteristic impedance zones can be observed in HWL line. The steady-state phase impedance can be measured with a small error in the first zone and the third zone. Faults in the second zone (the middle of line) introduce a very high deviation due to line transposition.

Keywords: Transmission line, half-wavelength, fault, impedance, resonance.

1. INTRODUCTION

In the recent years, there is an increase of transmission line projects with very long distance due to the necessity to transport energy from new resources or interconnect power system to exchange energy. Nowadays, these projects use HVDC (High Voltage Direct Current) technology due to great advance in power electronics and control systems. HVDC clearly has an advantage over classic HVAC (High Voltage Alternating Current) technology for distance between 500 to 1500 km, presenting better performance and even lower cost. However, for greater distances, bulk power transmission with HVDC begins to experience some undesirable phenomena that include the necessity and dependence of very heavy reactive power compensation [1], coarse voltage-reactive power control [2], commutation failures [3], high energization voltages and currents [4], among others, all of them due to power electronics converters and complex control system.

Half-wavelength (HWL) transmission line is an alternative for very long distance transmission that can offer flexibility to operate for distance higher than 1500 km [5]. It has been studied for many decades and it has outstanding steady-state operation properties due to its natural reactive power balance [6]. Additionally, HWL lines with optimized tower geometry can have competitive Right of Way (ROW) [7] regarding HVDC lines. Therefore, with similar ROW and the non-dependence on power electronics and their heavy reactive power compensation, HWL lines present lower cost than HVDC lines [8], and they are immune to the main problems experienced by HVDC lines.

Despite all these features, HWL technology is not in operation around the world. One of the main issues that HWL line experiences is the adequate comprehension of its behavior under fault condition. Due to its very long length, HWL line has different impedance characteristics. The line capacitance must not be neglected and it produces a different fault impedance behavior, and different voltage and current response under faults. This is because fault in some regions of HWL line produces network-frequency resonance [9]. The main problems of this phenomenon are severe overvoltage profile and large power excursion that can be adequately mitigated using resonance detuning systems [10]. However, the fact of having different impedance behavior prevents typical protection functions and algorithms of properly working for faults in HWL lines [11]. In addition, some issues about phasor estimation were reported due to different voltage and current behavior [12]. In the HWL line protection field, some studies introduce solutions for fault detection [13], fault phase selection and fault location [14] with promising results.

This paper analyzes the fault impedance on HLW lines to bring more insight on the effect of capacitance, the resonance phenomenon and the transmission line model in the process of impedance measurement in protective devices. As the steady-state ideal phase impedance, considering ideal transposition line and non-frequency dependent model, is usually used for impedance calculations to adjust protective devices, this paper study the deviation from ideal values caused by point of fault, transmission line model and phasor estimation process.

2. HWL TEST SYSTEM

2.1 HWL Transmission line

The test transmission line at 800 kV-60 Hz is slightly longer than the positive-sequence HWL, i.e., 2600 km. This line connects a generation station to a power grid (source-grid case). The tower design is optimized to increase the surge impedance loading (SIL-Pc) by modifying the bundle geometry, respecting constraints such as the maximum electric field on the conductor surface to avoid the corona effect and maximum electric field on the soil [7]. The ellipsoidal bundle geometry used is shown in Fig. 1 (average height). This configuration results in a considerable reduction in the UHVAC line right-of-way (ROW), comparable to that of HVDC lines. Line SIL is 4745 MW. The adopted soil resistivity is 2000 Ω.m. Table I shows the electrical parameters for 60 Hz, considering a balanced line.

2.2 Equivalent power system

The sending station has 11 synchronous machines with step-up transformers (T1), resulting in a three-phase short-circuit current (Scc) at the 800-kV busbar of 9.6 kA. The parameters of each machine are based on a real generation station (Serra da Mesa, Brazil). The receiving system is based on a strong Brazilian 500-kV electrical power system: 40 kA (strong point of connection). A step-down transformer (T2) of 800/500 kV is used to connect the HWL transmission line with the power system at the receiving end. Table II shows the system parameters.

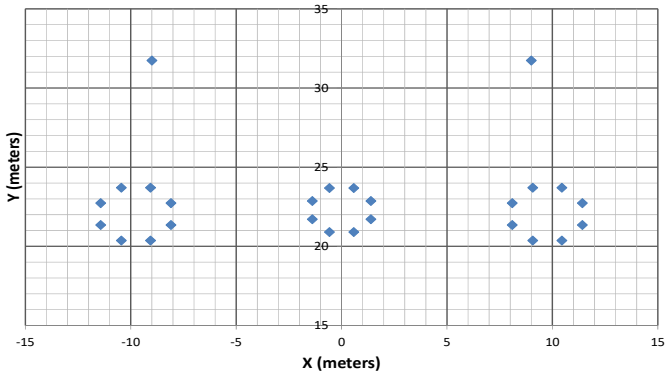

Fig. 1. Bundle geometry of HWL line.

TABLE I. Transmission line parameters at 60 Hz

Electrical parameters		
Zero sequence		
R0 (Ω /km)	X0 (Ω/km)	B0 (μS/km)
0.3871	1.3502	4.066
Positive/negative sequence		
R1 (Ω /km)	X1 (Ω /km)	B1 (μS/km)
0.0068	0.1737	9.5367
Electromagnetic parameters		
	Positive/Negative seq.	Zero seq.
$\gamma^{1\text{-}2}$ | γ^{0} (km^{-1})	0.0000254+j0.001287	0.0003356+j0.0024009
$Z^{1\text{-}2}{}_{C}$ | $Z^{0}{}_{C}$ (Ω)	134.98	572.68
$P^{1\text{-}2}{}_{C}$ (MW)	4745	---
$\lambda^{1\text{-}2}$ | λ^{0} (km)	4882	2616

TABLE II. Power system parameters

Source equivalent impedances				
Source	Zero Sequence (Ω)			
Generation – 15 kV	0.000342 + j 0.011775			
Strong System – 500 kV	7.2169 + j 36.084			
Source	Positive Sequence (Ω)			
Generation – 15 kV	0.000342 + j 0.011775			
Strong System – 500 kV	0.4801 + j 7.201			
Equivalent transformer				
Transformer	Xr (%)	kV	MVA	Connection
T1	11.84	800/15	5197.5	Yn / Δ
T2	10.00	800/500	4500.0	Yn /Yn

3. HWL FAULT IMPENDACE FEATURES

3.1 Series and shunt reactance of HWL line

To understand the fault impedance characteristic of HWL line it is important to observe the behavior of series impedance (Z_1) and shunt admittance (Y_1) of the positive sequence equivalent PI model of a long line calculated by Equations (1) and (2), where Z_C^1 is the characteristic impedance, γ^1 is the propagation constant (both for positive sequence) and d is the length line.

$$Z_1 = L_{(d)} = Z_C^1 \sinh(\gamma^1 d) \quad (1)$$

$$Y_1 = M_{(d)} = \frac{\tanh(\gamma^1 d/2)}{Z_C^1} \quad (2)$$

Fig. 2 shows the series and shunt reactance as a function of line length. Capacitive shunt reactance of line is greater than inductive series reactance for short lines (d<400 km). However, for longer lines capacitive and inductive reactances have similar values, especially for d >1200 km. There are two crossings of capacitive and inductive reactances, first at 1200 km and second at 2440 km (λ/2). Faults at these points of HWL line are prone to zero reactance conditions.

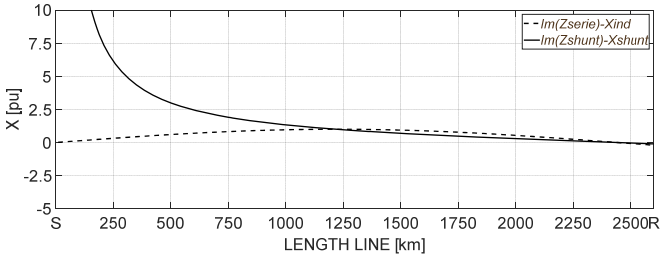

Fig. 2. Series and shunt reactance for hyperbolic (long) line model.

3.2 Fault impedance

The positive sequence fault impedance seen by equivalent Thevenin source at sending end was calculated for a three-phase low resistance fault (Rf=0.01Ω).

Fig. 3 shows the total resistance, reactance and impedance seen by the equivalent source at sending end. For faults applied up to 750 km the behavior of reactance is inductive and almost linear, and the resistance is linear with lower values. Further from this point, the reactance and resistance experiment a non-

linear behavior due to the proximity between series and shunt reactance line values, as shown in Fig. 2. There is a high increase in inductive reactance followed by a sudden decrease in total reactance for faults between 1000 and 1250 km, with a total reactance zero-crossing at 1210 km. Faults further from 1250 km produce an increase in reactance that stays capacitive up to 2160 km were a new zero crossing happens. The resistance experiments a great increase for faults between 1000 and 1210 km, and a decrease between 1210 and 1300 km.

Impedance seen by receiving source has similar characteristics, with slight difference due to Thevenin equivalent impedance of each source. As a result of this behavior, impedance seen from each source has three zones:

a. First zone: 0-1000 km with inductive reactance and resistance almost linear, similar to what is observed in conventional-length lines.

b. Second zone: 1000-1500 km, with non-linear reactance and a zero-crossing, and high total impedance due to high resistance values.

c. Third zone: 1500-2600 km with capacitive reactance and resistance almost linear. In this region, a resonant condition with low reactance and low resistance is observed for fault around 2160 km.

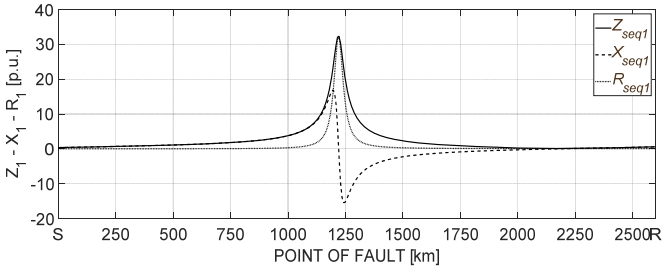

Fig. 3. Total fault impedance seen by sending source.

3.3 Ideal phase impedance at HWL terminals

Protective devices calculate line impedance based on voltage and current measurements on line terminals. Typically, there are two ways to calculate impedance:

a. Phase impedances are obtained from the division of line voltage and the respective variation of phase currents. They are considered to detect line-to-line faults.

b. Phase to ground impedance are obtained from a division of the phase voltage and the respective phase currents adequately compensated. They are used to detect line to ground (LG) faults.

Classical line to ground impedance compensation does not consider shunt capacitance. However, even when the capacitive affect is considered (long line correction) it does not work properly for lines with HWL length [15]. Zero sequence and negative sequence quantities and directionality seem to be a better methodology to deal with LG fault detection in very long distance transmission lines. In this paper we will focus on phase impedance to detect line-to-line (LL) faults.

3 .4 R-X diagram of ideal phase impedance

Three-phase system was evaluated using two-port network in order to calculate phase impedance for different type of faults symmetrical and asymmetrical). Fig. 4 shows the single-line diagram of equivalent test system. The equivalent ABCD matrix of the system equation is given by (3). Voltage at sending and receiving ends are set to pre-fault values. The internal currents of the sending and receiving sources are calculated by Equation (4). For this section the transmission line is considered ideally transposed (balanced line).

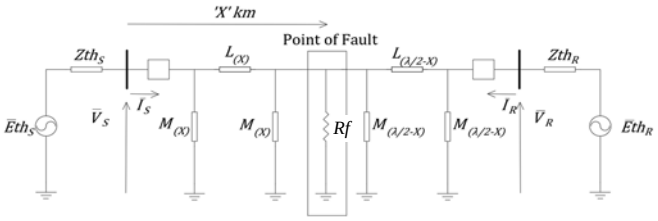

Fig. 4. Single-line diagram of equivalent system.

$$[Q_{eq}] = [Q_{ZeqS}][Q_{L(X)}][Q_{Fault}]\left[Q_{L\left(\frac{\lambda}{2}-X\right)}\right][Q_{ZeqR}] \quad (3)$$

$$\begin{bmatrix}\bar{V}_{Sabc}\\ \bar{I}_{Sabc}\end{bmatrix} = [Q_{eq}]\begin{bmatrix}\bar{V}_{Rabc}\\ \bar{I}_{Rabc}\end{bmatrix} \quad (4)$$

where:
Q_{eq}: two-port network impedance matrix of three-phase system including an equivalent system at the sending end, a HWL line with fault and an equivalent system at the receiving end;
Q_{ZeqS}: two-port network impedance matrix of the three-phase equivalent system at the sending end;
$Q_{L(X)}$: two-port network impedance matrix of the three-phase segment of the line with X km;
Q_{Fault}: two-port network sequence matrix of the fault;
$Q_{L(\lambda/2-X)}$: two-port network impedance matrix of the three-phase segment of the line with $\lambda/2 - X$ km;
Q_{ZeqR}: two-port network impedance matrix of the three-phase equivalent system at the receiving end;
$\bar{V}_{Sabc}$, $\bar{I}_{Sabc}$: vector of the internal phase voltage and current at the sending equivalent system;
$\bar{V}_{Rabc}$, $\bar{I}_{Rabc}$: vector of the internal phase voltage and current at the receiving equivalent system.

Using two-port network methodology voltage, current and phase impedance at sending and receiving terminals of HWL line under fault in different points were calculated. Fig. 5 shows the magnitudes of voltage and current at line terminals as a function of fault location. It can be observed that voltage and current have a different behavior in the fault impedance zones defined in section 3.2. The first zone (0-1000 km) voltage at sending terminal increases and the current decreases as fault moves away from the terminal due to the inductive behavior of fault impedance. In the central region, between 1000 – 1500 km, the current at sending terminal has lower value (up to 0.02 pu around 1200 km) and the voltage magnitude is around 1.0 pu, showing a high fault impedance behavior.

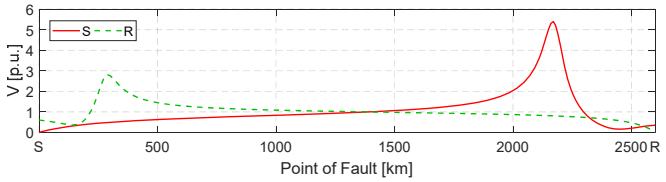

a.Voltage

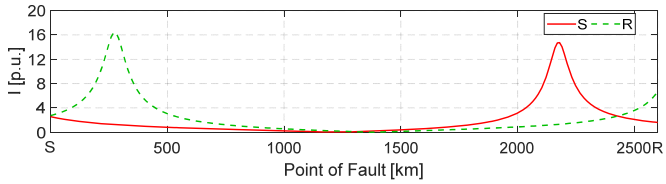

b.Current

Fig. 5. Voltage and current at sending and receiving ends

In the third zone the voltage at sending terminal continue to increase, reaching the highest value around 2160 km due to a resonance condition for fault at that point. There are small differences between the behavior of current and voltage of sending (S) and receiving (R) terminal, especially in the resonant point because of the terminal equivalents.

Fig. 6 shows the R-X diagram of AB impedance seen by sending and receiving terminal sources. Fault impedances were calculated with a resolution of 20 km along the line and only some points of fault (700, 1000, 1100, 1200, 1250, 1300, 1350, 1400, 1500, 1600, 1900 and 2600 km) are shown. The R-X diagram shows that impedance performs a circle. The larger part of impedance locus (circle) represents faults between 1100 km to 1500 km (20% of line length) that corresponds to the region with high impedance observed in Fig. 3. Faults between 0 to 1000 km and 1500 to 2600 km (80% of line length) depict an almost linear region in the first and fourth quadrant of R-X diagram.

4. HWL FAULT IMPEDANCE CALCULATION

In this section the steady-state fault impedance seen by relays are calculated in time-domain simulations using a Fast Fourier Transformation (FFT) and considering the effect of transmission line model and the point of fault. All calculations were simulated with PSCAD/EMTDC software.

4.1 Transmission line model

The following model cases are considered:

a. Bergeron model with ideal transposition (TIBE).

b. Bergeron model with real transposition (TRBE).

c. Frequency dependent model (Universal model) with ideal transposition (TIDF).

d. Frequency dependent model with real transposition (TRDF).

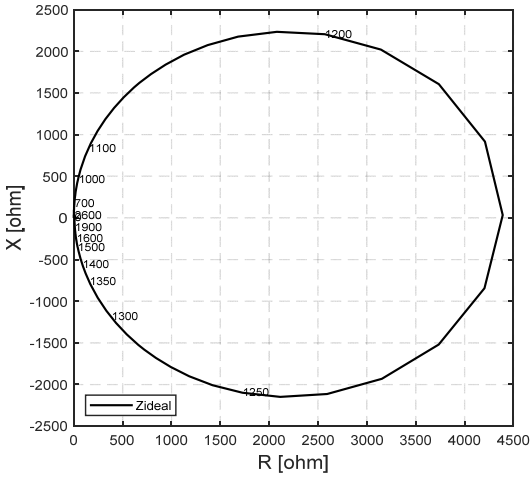

a.Sending end

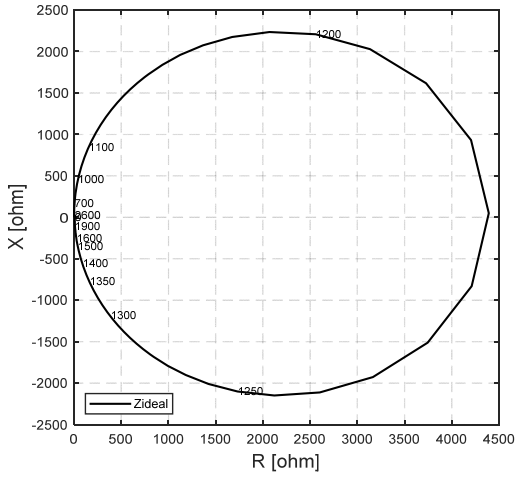

c. Receiving end

Fig. 6. R-X diagram of fault impedance at terminal ends.

For real transposition, there were considered 9 transposition cycles of 288 km each one. One cycle has a regular configuration of four subsections (1/6-1/3-1/3-1/6). Therefore, HWL line is split in 36 subsection that are also used to apply the 37 faults along the line.

4.2 Voltage and current phasor estimation

The voltage and current phasors simulated in PSCAD/EMTDC are calculated using FFT filter that includes a low pass filter (anti-aliasing). Computations of fundamental frequency components are based on a sampled data window of the preceding input signal cycle, considering 16 samples per cycle.

4.3 Steady-state phase impedance estimation

Impedance seen by the relay is calculated from three-phase faults simulations as a division of line voltage and the respective difference of phase currents. In order to obtain the steady-state impedance, the data were collected after 1 s.

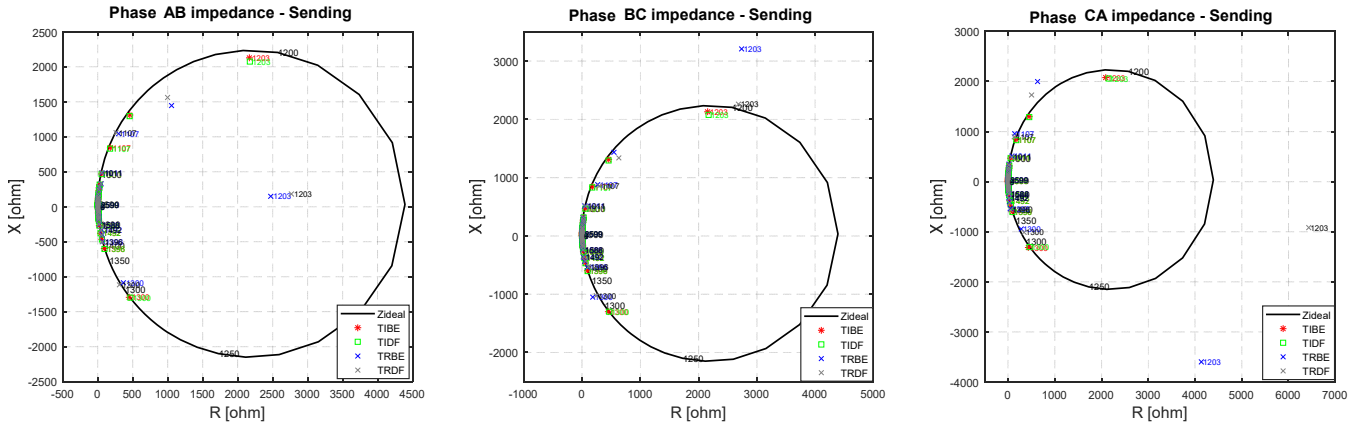

a. Sending end

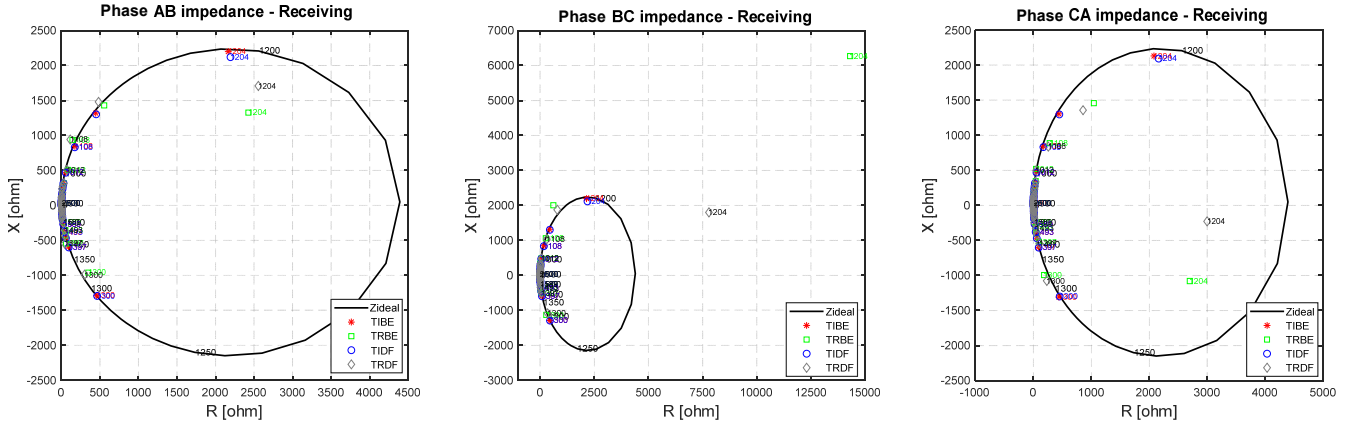

b. Receiving end

Fig. 7. X-R diagram of fault impedance for different line model.

5. STEADY-STATE IMPEDANCE RESULTS

Fig. 7 shows steady-state phase impedance calculated for different transmission line model and compared with ideal phase impedance for faults along the HWL. In this paper we analyze the deviations from ideal steady-state phase impedance considering transmission line model, transposition representation, point of fault and the digital phasor estimation process. At a glance, from Fig. 7, phase impedance estimated in the first zone (0-1000 km) and in the third zone (1500-2600 km) are similar to ideal values. However, higher differences from ideal values are found in the second zone, especially between 1200-1300 km for transmission line models with real transposition representation. This occurs because faults at central zone produce very low current values that are strong influenced by the unbalance introduced by transpositions. On the other hand, in this central region ideal transposition presents lower deviation from ideal phase impedance.

To observe more carefully the first and third zone, Fig. 8 shows a zoom of R-X diagram in the first zone impedance seen by receiving terminal and the third zone impedance seen by sending terminal. In the first zone, lower deviation from ideal impedance are presented with ideal transposition models. Real transposition models introduce a slightly higher deviation and also the values oscillate around ideal values due to transposition points. In the third zone, in a similar way, lower deviation from ideal impedance are presented with ideal transposition models. Real transposition models introduce slightly higher deviations and also those values oscillate around ideal values.

Table 3 shows the maximum deviation from ideal impedance values for different line models at different points of faults. In general, the phase impedance estimation suffers higher deviation from ideal values for faults further from terminals, and transposition introduces an additional deviation. Faults in the central line zone introduce higher deviation, especially when real transposition is considered. Disregarding frequency dependence of transmission line parameters introduces only a small deviation from ideal impedance values.

Table 3. Maximum deviation from ideal impedance

Point of Fault	Δ(I-TIBE) %	Δ(I-TIDF) %	Δ(I-TRBE) %	Δ(I-TRDF) %
289 km	1.3	1.3	1.4	1.6
578 km	1.5	1.6	1.6	1.8
1011 km	2.6	2.9	7.0	5.9
1204 km	21.2	20.3	46.6	73.8
1300 km	10.8	10.9	21.1	15.4
1500 km	7.5	7.1	9.9	6.3
2160 km	2.8	3.1	16.7	13.3
2600 km	9.4	9.7	22.7	11.3

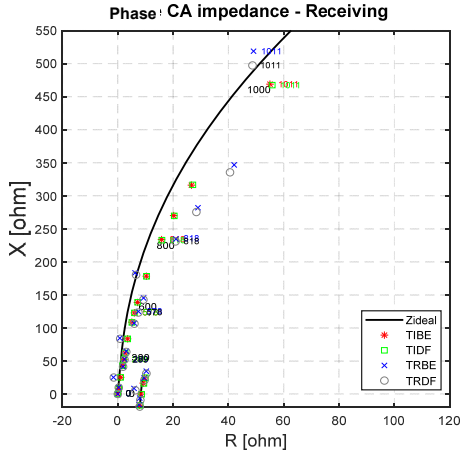

a. First zone seen by receiving end

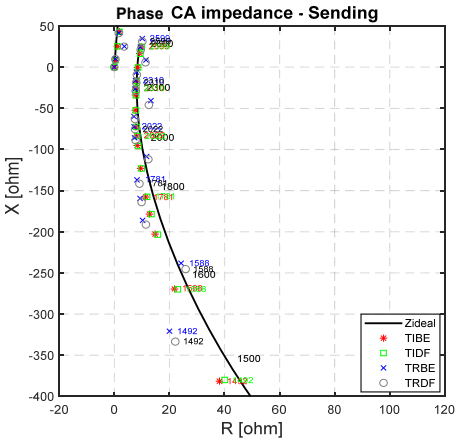

b. Third zone seen by sending end

Fig. 8. X-R diagram in the first and third zone.

6. CONCLUSIONS

This paper presents a study of phase impedance estimation in Half-Wavelength (HWL) lines under fault. First, it is found that faulted phase impedance has a different behavior in this very long line caused by the series inductive reactance and shunt capacitive reactance of line having two zero-crossing, the former at quarter-wavelength position and the other near to the half-wavelength position. Three characteristic impedance zones are observed: the first zone (0-1000 km) with inductive reactance and resistance almost linear; the second zone (1000-1500 km) with non-linear reactance that comprises the reactance zero-crossing and presents very high resistance; and the third zone (1500-2600 km) with capacitive reactance and resistance almost linear, which includes a resonant condition with low impedance at 2160 km. The deviations from steady-state ideal phase impedance characteristics are introduced by transmission line model, transposition representation, point of fault and digital phasor estimation process (Fast Fourier Transformation). The phase impedance suffers higher deviation from ideal values for faults further from terminals, and transposition introduces an additional deviation. Faults in the central zone of the line introduces higher deviation, especially when real transposition is considered. The estimation of fault impedance in the first zone (0-1000 km) can have a maximum deviation of 7% from ideal impedance. In the middle of the line, the line transposition does not allow a correct estimation of fault impedance, introducing up to 73% of deviation. In the third zone, the impedance can be measured with a maximum deviation of 9%. Faulted phase impedance can be measured with acceptable error in the first zone and the third zone, however transient analysis must be performed to assure a fast and correct performance of protective devices in these zones.

ACKNOWLEDGMENT

This work was supported by CAPES (code 001) and FAPESP (2017/20010-1), Brazil.

REFERENCES

[1] M. P. Bahrman and B. K. Johnson, “The ABCs of HVDC transmission technologies,” *IEEE Power Energy Mag.*, vol. 5, no. 2, pp. 32–44, 2007.

[2] P. McKeever and C. Ng, “Next generation HVDC network for offshore renewable energy industry,” in *10th IET International Conference on AC and DC Power Transmission (ACDC 2012)*, 2012, pp. 11–11.

[3] C. Guo, C. Li, C. Zhao, X. Ni, K. Zha, and W. Xu, “An Evolutional Line-Commutated Converter Integrated with Thyristor-Based Full-Bridge Module to Mitigate the Commutation Failure,” *IEEE Trans. Power Electron.*, vol. 32, no. 2, pp. 967–976, 2017.

[4] A. R. M. Tenório, K. S. Herszterg, D. R. Parrini, K. A. T. Carvalho, and A. F. C. Aquino, “Energizações dos Transformadores Conversores do Primeiro Bipolo de ±800 kV das Américas,” in *XIV SYMPOSIUM OF SPECIALISTS IN ELECTRIC OPERATIONAL AND EXPANSION PLANNING*, 2018, p. 13.

[5] J. S. Ortega and M. C. Tavares, “New perspectives about AC Link based on Half-Wavelength Properties for Bulk Power Transmission with Flexible Distance,” *IET Gener. Transm. Distrib.*, vol. 12, no. 12, pp. 3005–3012, 2018.

[6] F. Iliceto and E. Cinieri, “Analysis of half-wave length transmission lines with simulation of corona losses,” *IEEE Trans. Power Deliv.*, vol. 3, no. 4, pp. 2081–2091, 1988.

[7] J. S. Acosta and M. C. Tavares, “Methodology for optimizing the capacity and costs of overhead transmission lines by modifying their bundle geometry,” *Electr. Power Syst. Res.*, vol. 163, no. Part B, pp. 668–677, Oct. 2017.

[8] G. Samorodov *et al.*, “Technical and economic comparison between direct current and half-wavelength transmission systems for very long distances,” *IET Gener. Transm. Distrib.*, vol. 11, no. 11, pp. 2871–2878, 2017.

[9] J. Santiago and M. C. Tavares, “Analysis of half-wavelength transmission line under critical balanced faults: Voltage response and overvoltage mitigation procedure,” *Electr. Power Syst. Res.*, vol. 166, no. October 2018, pp. 99–111, 2019.

[10] J. S. Ortega and M. C. Tavares, “Transient Analysis and Mitigation of Resonant Faults on Half-Wavelength Transmission Lines,” *Trans. Power Deleivery - IEEE (In Rev.*, pp. 1–8, 2019.

[11] R. G. Fabián and M. C. Tavares, “Using of Conventional Relays for Protecting Half-Wavelength Transmission Line from Three-Phase Faults,” in *International Conference on Power Systems Transients 2013*, 2013.

[12] B. F. Kusel, K. M. Silva, and E. C. Molas, “Analysis of phasor estimation in signals from faults in Half-wave length transmission lines,” in *Anais do XIS Congresso Brasildeiro de Automatica*, 2012, pp. 4588–4595, Campina Grande, Brazil.

[13] R. G. Fabián, “Distance Protection for Half-Wavelength Power Transmission Lines (In Portuguese),” Doctoral Thesis, University of Campinas, Brazil, 2015.

[14] F. V. Lopes, B. F. Küsel, K. M. Silva, D. Fernandes, and W. L. A. Neves, “Fault location on transmission lines little longer than half-wavelength,” *Electr. Power Syst. Res.*, vol. 114, pp. 101–109, 2014.

[15] A. G. De Castro, L. A. Soares, M. R. Araujo, W. B. F. Drumond, A. L. M. Coelho, and I. P. Faria, “Performance analysis of non-conventional distance protection and phase selection algorithms in transmission lines little longer than half- wavelength,” in *2018 13th IEEE International Conference on Industry Applications, INDUSCON 2018 - Proceedings*, 2019, pp. 1008–1015.